Transp Porous Med (2011) 89:121–134
DOI 10.1007/s11242-011-9758-1

Macrodispersion by Point-Like Source Flows in Randomly Heterogeneous Porous Media

Gerardo Severino

Received: 25 August 2010 / Accepted: 25 March 2011 / Published online: 8 April 2011

Abstract A pulse of a passive tracer is injected in a porous medium via a point-like source. The hydraulic conductivity K is regarded as a stationary isotropic random space function, and we model macrodispersion in the resulting migrating plume by means of the second-order radial spatial moment X_{rr}. Unlike previous results, here X_{rr} is analytically computed in a fairly general manner. It is shown that close to the source macrodispersion is enhanced by the large local velocities, whereas in the far field it drastically reduces since flow there behaves like a mean uniform one. In particular, it is demonstrated that X_{rr} is bounded between X_∞ corresponding to the short-range (far field), and X_0 pertaining to the long-range (near-field) correlation in the conductivity field. Although our analytical results rely on the assumption of isotropic medium, they enable one to grasp in a simple manner the main features of macrodispersion mechanism, therefore providing explicit physical insights. Finally, the proposed model has potential toward the characterization of the spatial variability of K as well as testing more general numerical codes.

Keywords Porous media · Point-like source flow · Heterogeneity · Macrodispersion · Stochastic modeling

1 Introduction

Advection of a passive tracer in heterogeneous porous media arises in a variety of settings such as flows through fixed-bed catalytic reactors and the migration of pollutants in the subsurface. Due to the erratic variations of the hydraulic conductivity K the advection dispersion equation

G. Severino (✉)
Division of Water Resources Management, University of Naples Federico II,
via Università 100, 80055 Portici, NA, Italy
e-mail: gerardo.severino@unina.it

G. Severino
Department of Mechanical and Aerospace Engineering (MAE), University of California,
9500 Gilman Drive EBU II, Mail Code 0411 La Jolla, San Diego, CA 92093, USA

(ADE), describing the evolution of the tracer concentration, becomes inhomogeneous. One way to deal with the inhomogeneous ADE is by means of a perturbation approach. The basic idea is to start from the homogeneous version of the problem (which usually is solvable). Subsequently, the homogeneous solution is perturbed by regarding $K = K(\mathbf{x})$ as a random space function (RSF). Hence, the appropriate quantities (i.e., spatial/temporal moments of the concentration field, and breakthrough curves) are expressed as expansions involving the statistical properties of K.

In the present paper, we are motivated by the particular case of tracer dispersion in geological media such as aquifers and hydrocarbon reservoirs. A considerable amount of experimental data, theoretical modeling, and physical insight is available, but largely for situations where flow is uniform in the mean (a comprehensive review can be found in Dagan 1989 and Rubin 2003). However, in many settings (such as pump and treat remediation-strategies, forced-gradient transport experiments, etc.) the mean flow is more likely to be radial than uniform. Typically, fluid is pumped in the formation by an injection well, and recovered from one (or more) extracting well(s). Since wells generally partially penetrate the medium, their length may result much smaller than the characteristic size of the flow domain. Thus, wells are likely to be modeled as point-like source/sink terms.

The aim here is to investigate advective transport by a point-like source-flow. This is achieved by employing a perturbation expansion which regards the normalized fluctuation $\varepsilon(\mathbf{x}) = 1 - \frac{K(\mathbf{x})}{K_\mathrm{A}}$ (being K_A the arithmetic mean of K) as an isotropic RSF . Unlike previous studies on the same topic (e.g., Indelman and Dagan 1999), we derive a general analytical expression for the second-order radial spatial moment. This enables one to better quantify the spreading mechanism of tracers as well as the differences with results based on the approximation proposed by Indelman and Dagan 1999. Finally, our analytical results represent an useful tool to characterize (by means of tracer tests) the spatial (statistical) structure of the conductivity field and to check more sophisticated numerical codes, the assumption of isotropy notwithstanding.

2 Problem Statement and Phenomenological Assumptions

A three-dimensional porous medium lies in an unbounded domain Ω. The conductivity $K(\mathbf{x})$ is modeled as a stationary RSF with mean K_A, and given isotropic autocorrelation function $\rho(x)$ (whose correlation integral scale will denoted by I). Steady-state flow is generated by a point-like injection of water at constant volumetric rate Q. The governing equations are the constitutive (Darcy) model, and the mass conservation law

$$\mathbf{q}(\mathbf{x}) = K(\mathbf{x})\mathbf{E}(\mathbf{x}), \qquad \nabla \cdot \mathbf{q} = Q\,\delta(\mathbf{x}) \qquad (\mathbf{x} \in \Omega), \tag{1}$$

respectively. In Eq. 1, $\mathbf{q}(\mathbf{x})$ is the flux, and $\mathbf{E}(\mathbf{x}) = -\nabla\Phi(\mathbf{x})$ represents the gradient of the potential Φ. In the case of a line-like source flow, which is adopted to model well flows (Indelman et al. 1996), the constant head boundary condition on the well is the most appropriate. However, results valid for transport generated by a point-like source flow can be approximately applied to those (partially penetrating) wells which are short enough as compared with the characteristic size of the flow domain (see discussion in Indelman and Dagan 1999). In addition, Severino et al. (2008) have shown that in the case of diverging radial flows (like the one considered here) the difference due to different boundary conditions at the source is significant only within a distance from the source of a few integral scales. As a consequence, although the condition of prescribed flux at the source is in principle not

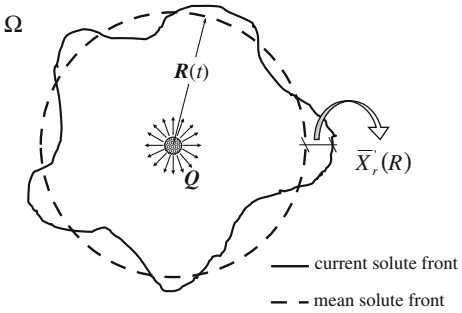

Fig. 1 Definition sketch for solute spreading by a point-like source flow (horizontal cross-section) taking place in the domain Ω. Continuous line represents the current (i.e., one realization) solute front, whereas $\overline{X}_r'$ is the trajectory fluctuation around the mean front (dashed line), which is given by the deterministic relationship $R = R(t)$

appropriate for flows toward a fully penetrating well, it is still applicable to: (i) partially penetrating wells (which are short enough) and (ii) diverging radial flows.

Elimination of $\mathbf{q}(\mathbf{x})$ in (1) leads to

$$\nabla \cdot [K(\mathbf{x}) \nabla \Phi(\mathbf{x})] = -Q\,\delta(\mathbf{x}). \tag{2}$$

The solution of the stochastic Poisson-type Eq. 2 yields the RSF $\Phi(\mathbf{x})$, and subsequently the flux $\mathbf{q}(\mathbf{x})$ (via the Darcy model). As for transport, the concentration (solute mass per liquid volume) $C(\mathbf{x}, t)$ satisfies the ADE

$$\frac{\partial}{\partial t} C + \mathbf{U} \cdot \nabla C = \nabla \cdot (\mathbf{D} \nabla C), \tag{3}$$

where $\mathbf{U} = \frac{\mathbf{q}}{n}$ is the fluid velocity, n the formation porosity (assumed constant), and $\mathbf{D}$ is the pore-scale dispersion. Due to the spatial variations of K, the velocity $\mathbf{U}$ fluctuates along flow paths, and concurrently the tracer-plume develops with an irregular structure (Fig. 1). Our main aim is the computation of the second-order radial spatial moment of the migrating plume, which characterizes the macrodispersion mechanism.

The problem stated here in a general form is computationally difficult (for a wide discussion concerning the various technical aspects, see Indelman and Dagan 1999). A simple solution can be achieved by adopting a few assumptions: (i) a first-order approximation in $\sigma^2 = \langle \varepsilon^2(\mathbf{x}) \rangle$ (appropriate for mildly heterogeneous formations) is used to compute the potential $\Phi(\mathbf{x})$; (ii) pore-scale dispersion is neglected, i.e., $D = 0$. Indeed, it is known that $\mathbf{D}$ has a minor impact on the macrodispersivity as compared to advection (e.g., Lessoff and Indelman 2004). The assumptions (i) and (ii) enable one to reduce the mathematical complexity, while keeping the salient features of the problem at stake. Also the assumption of isotropy is not very limiting since macrodispersivity is less sensitive to the anisotropy both in transport by groundwater (see e.g., Dagan 1989) and in transport by source-flows (Indelman and Dagan 1999).

3 Velocity Covariance

We compute here the two-point velocity covariance, since it will be instrumental for macrodispersion modeling. Thus, we introduce the zero mean RSF $\varepsilon(\mathbf{x})$ defined as

$$\varepsilon(\mathbf{x}) = 1 - \frac{K(\mathbf{x})}{K_A}, \tag{4}$$

and substitute into (2), to have

$$\Delta\Phi(\mathbf{x}) = -\nabla\cdot[\varepsilon(\mathbf{x})\mathbf{E}(\mathbf{x})] - \frac{Q}{K_{\mathrm{A}}}\delta(\mathbf{x}). \tag{5}$$

In order to solve Eq. 5, the potential is expanded in an asymptotic series

$$\Phi(\mathbf{x}) = \sum_i \Phi^{(i)}(\mathbf{x}), \qquad \Phi^{(i)} = \mathrm{O}(\varepsilon^i). \tag{6}$$

Substituting into (5), and collecting the same order terms, leads to

$$\Delta\Phi^{(0)}(\mathbf{x}) = -\frac{Q}{K_{\mathrm{A}}}\Delta(\mathbf{x}), \quad \Delta\Phi^{(i)}(\mathbf{x}) = -\nabla\cdot\left[\varepsilon(\mathbf{x})\mathbf{E}^{(i-1)}(\mathbf{x})\right], \quad i = 1, 2, .. \tag{7}$$

where $\Phi^{(0)}(x) = \frac{Q}{K_{\mathrm{A}}}G(x)$ represents the solution pertaining to a homogeneous formation, whereas $G(x) = \frac{1}{4\pi x}$ is the Green function. The fluctuation $\Phi^{(1)}(\mathbf{x})$ of the potential is expressed as

$$\Phi^{(1)}(\mathbf{x}) = \frac{Q}{K_{\mathrm{A}}}\int_{\Omega} \mathrm{d}\mathbf{x}'\varepsilon(\mathbf{x}')\frac{\partial}{\partial x'_m}G(x')\frac{\partial}{\partial x'_m}G(|\mathbf{x}-\mathbf{x}'|) \qquad m = 1, 2, 3. \tag{8}$$

Substitution of (4) into the constitutive model, and applying the perturbation expansion yields the mean value, and fluctuation of the velocity:

$$\langle U(x)\rangle = \frac{K_{\mathrm{A}}}{n}E^{(0)}(x), \qquad \mathbf{u}(\mathbf{x}) = \frac{K_{\mathrm{A}}}{n}\left[\mathbf{E}^{(1)}(\mathbf{x}) - \varepsilon(\mathbf{x})\mathbf{E}^{(0)}(\mathbf{x})\right], \tag{9}$$

respectively. The two-point velocity covariance $u_{l,m}(\mathbf{x},\mathbf{y}) = \langle u_l(\mathbf{x})u_m(\mathbf{y})\rangle$ is now written as $u_{l,m}(\mathbf{x},\mathbf{y}) = \left(\frac{K_{\mathrm{A}}}{n}\right)^2\overline{u}_{l,m}(\mathbf{x},\mathbf{y})$, being

$$\overline{u}_{l,m}(\mathbf{x},\mathbf{y}) = \left(\frac{\sigma}{\chi}\right)^2\frac{x_l y_m}{(xy)^3}\rho(|\mathbf{x}-\mathbf{y}|) - \frac{1}{\chi}\widetilde{u}_{l,m}(\mathbf{x},\mathbf{y}) + C_{E_lE_m}(\mathbf{x},\mathbf{y}) \quad \left(\chi = \frac{4\pi K_{\mathrm{A}}}{Q}\right) \tag{10}$$

$$\widetilde{u}_{l,m}(\mathbf{x},\mathbf{y}) = \frac{x_l y_m}{xy}\left[\frac{1}{x^2}\frac{\partial}{\partial y}C_{\varepsilon\Phi}(\mathbf{x},\mathbf{y}) + \frac{1}{y^2}\frac{\partial}{\partial x}C_{\varepsilon\Phi}(\mathbf{y},\mathbf{x})\right] \qquad l, m = 1, 2, 3. \tag{11}$$

The quantity $C_{E_lE_m}(\mathbf{x},\mathbf{y}) = \left\langle\frac{\partial}{\partial x_l}\Phi^{(1)}(\mathbf{x})\frac{\partial}{\partial y_m}\Phi^{(1)}(\mathbf{y})\right\rangle$ represents the potential-gradient covariance, whereas $C_{\varepsilon\Phi}(\mathbf{x},\mathbf{y}) = \left\langle\varepsilon(\mathbf{x})\Phi^{(1)}(\mathbf{y})\right\rangle$ is the cross-correlation between ε, and the potential Φ. The decomposition (10) is justified by the fact that one can clearly distinguish the contributions (i.e., $\widetilde{u}_{l,m}$ and $C_{E_lE_m}$) due to the fluctuations of the potential gradient from the quantity $\left(\frac{\sigma}{\chi}\right)^2\frac{x_l y_m}{(xy)^3}\rho(|\mathbf{x}-\mathbf{y}|)$ which instead is due to the mean head gradient. In particular, since far away from the source the head gradient fluctuation is practically immaterial (because of the vanishing effect of the boundary condition at the source), one has

$$u_{l,m}(\mathbf{x},\mathbf{y}) \simeq \left(\frac{Q\sigma}{4\pi n}\right)^2\frac{x_l y_m}{(xy)^3}\rho(|\mathbf{x}-\mathbf{y}|) \qquad (x, y \gg I), \tag{12}$$

solely. The velocity covariance $u_{l,m}$ has been derived (see the "Appendix" for details) for any autocorrelation ρ, and the final result reads as:

$$u_{l,m}(\mathbf{x},\mathbf{y}) = \left(\frac{\overline{Q}}{4\pi}\right)^2 \frac{x_l y_m}{xy}\left[\frac{\rho(x-y)}{(xy)^2} + \frac{4}{x}\Psi(x,y) + \frac{2}{y}\Psi(y,x)\right] \qquad \left(\overline{Q} = \frac{Q}{n}\sigma\right) \tag{13}$$

$$\Psi(x,y) = \int_x^\infty \frac{d\xi\,\xi^2\rho(\xi)}{\left[\xi^2 - x(x-y)\right]^3} + \int_{-(x-y)}^\infty \frac{d\xi\,\xi^2\rho(\xi)}{\left[\xi^2 - x(x-y)\right]^3} - \int_{x-y}^\infty \frac{d\xi\,\xi^2\rho(\xi)}{\left[\xi^2 - x(x-y)\right]^3}. \tag{14}$$

The velocity variance is

$$\sigma_u^2(x) = \left(\frac{\overline{Q}}{2\pi x^2}\right)^2 \left[1 + \frac{3}{2}\psi(x)\right], \qquad \psi(x) = x^3 \int_x^\infty \frac{d\xi}{\xi^4}\rho(\xi). \tag{15}$$

Since it yields

$$\psi(0) = \frac{\rho(0)}{3} = \frac{1}{3}, \qquad \psi(\infty) = \frac{\rho(\infty)}{3} = 0, \tag{16}$$

the following asymptotics for $\sigma_u^2(x)$ are easily established

$$\sigma_u^2(0) = \infty, \qquad \sigma_u^2(\infty) = 0. \tag{17}$$

Indeed, close to the source the flow behaves as one taking place in a homogeneous medium with constant (harmonic) conductivity K_{H} (Shvidler 1985). As a consequence, the local velocity $U(x)$ is proportional to x^{-2}, and therefore singular at the source. At the other extreme of large distances the flow behaves as a homogeneous one (generated by the effective conductivity K^{eff}), and thus the velocity variance vanishes in the far field. These asymptotics are in agreement with the numerical simulations of Naff (1991).

To better address the uncertainty of the velocity field, it is convenient to consider the coefficient of variation $\mathrm{CV}_u(x) = \frac{\sigma_u(x)}{\langle U(x)\rangle}$ which is given by:

$$\mathrm{CV}_u(x) = 2\sigma\left[1 + \frac{3}{2}\psi(x)\right]^{1/2}. \tag{18}$$

Based on the asymptotics (17), it is easily seen that

$$\mathrm{CV}_u(0) = \sqrt{6}\,\sigma, \qquad \mathrm{CV}_u(\infty) = 2\,\sigma. \tag{19}$$

Thus, both in the near and far field the variance $\sigma_u^2(x)$ behaves like $\langle U(x)\rangle^2$. The condition $\mathrm{CV}_u(\infty) < \mathrm{CV}_u(0)$ is explained by the very large variations of local velocities at the source, whereas in the far field the flow is slowly varying. Furthermore, because of the conditioning effect due to the fixed (i.e., given volumetric rate Q) boundary condition at $x = 0$, close to the source velocities are highly correlated whereas they become uncorrelated as x increases. As it will be clearer later on, this finding is of paramount importance when analyzing the macrodispersion evolution. Finally, it is worth underlying here that the asymptotics (19) represent an useful information for some practical applications, such as the identification of the formation heterogeneity structure (see discussion in Indelman 2001).

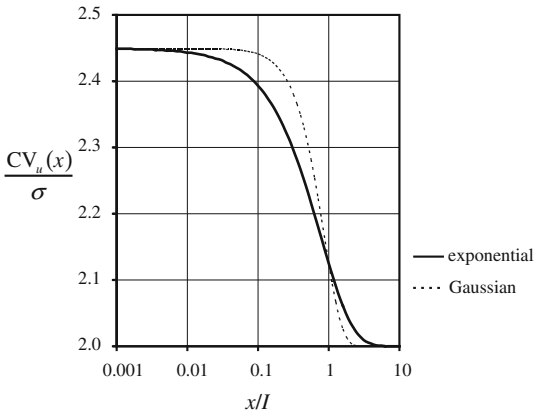

Fig. 2 Scaled velocity coefficient of variation $\frac{\mathrm{CV}_u(x)}{\sigma}$ versus the normalized distance from the source

The transitional regime of (18) is evaluated after computing $\psi(x)$ for given ρ. By assuming exponential, i.e., $\rho(x) = \exp(-x)$, and Gaussian, i.e., $\rho(x) = \exp\left(-\frac{\pi}{4}x^2\right)$, model leads to

$$\psi(x) = \frac{1}{6}\begin{cases} (2 - x + x^2)\exp(-x) + x^3\,\mathrm{Ei}(-x) & \text{(exponential)} \\ (2 - \pi x^2)\exp\left(-\frac{\pi}{4}x^2\right) + \frac{\pi^2}{2}x^3\,\mathrm{erfc}\left(\frac{\sqrt{\pi}}{2}x\right) & \text{(Gaussian)} \end{cases} \tag{20}$$

(we have considered the length x normalized by I, although for simplicity we have retained the same notation). The scaled coefficient of variation $\frac{\mathrm{CV}_u(x)}{\sigma}$ versus the normalized distance from the source is depicted in Fig. 2. At small distances $\frac{\mathrm{CV}_u(x)}{\sigma}$ is less persistent for exponential ρ, whereas it decreases (with increasing x) faster for Gaussian ρ. This is quantitatively demonstrated by the following expansions

$$\frac{\mathrm{CV}_u(x)}{\sigma} = \begin{cases} \sqrt{6} + \mathrm{O}(x) & \text{(exponential)} \\ \sqrt{6} + \mathrm{O}(x^2) & \text{(Gaussian)} \end{cases} \qquad x \ll I, \tag{21}$$

and

$$\frac{\mathrm{CV}_u(x)}{\sigma} = \begin{cases} 2 + \mathrm{O}(x^{-1}) & \text{(exponential)} \\ 2 + \mathrm{O}(x^{-2}) & \text{(Gaussian)} \end{cases} \qquad x \gg I. \tag{22}$$

Finally, it is seen that the far field $\mathrm{CV}_u(\infty)$ is achieved after ten correlation scales.

4 Macrodispersion Analysis

Macrodispersion is modeled by means of the second-order radial spatial moment $X_{rr}(R)$ that is equal to the variance $\langle \overline{X}_r'^2(R)\rangle$ of the particle trajectory $X_r(R)$. At the first-order in σ^2, the fluctuation of $X_r(R)$

$$\overline{X}_r'(R) = X_r(R) - \langle X_r(R)\rangle \tag{23}$$

(see also Fig. 1) is computed as follows (for the general framework, see Indelman and Rubin 1996):

$$\frac{\mathrm{d}}{\mathrm{d}t}\overline{X}_r' - \overline{X}_r'\frac{\partial}{\partial R}\langle U(R)\rangle = u_{\mathrm{r}}(t), \qquad \langle U(R)\rangle = \frac{\mathrm{d}}{\mathrm{d}t}R = \frac{Q}{4\pi n R^2}, \tag{24}$$

where u_{r} represents the fluctuation of the velocity along the radial direction. The second of (24) is solved straightforwardly with zero initial condition, to give

$$R\,(t) = \left(\frac{3\,Qt}{4\,\pi n}\right)^{1/3}. \tag{25}$$

To compute the fluctuation $\overline{X}_r'$ it is convenient to switch to R as independent variable, and to make use of (25) to yield

$$\overline{X}_r'\,(R) = \frac{4\pi n}{QR^2}\int_0^R \mathrm{d}x\, x^4 u_r(x). \tag{26}$$

The trajectory variance is now calculated as

$$X_{rr}(R) = \left(\frac{4\pi n}{QR^2}\right)^2 \int_0^R\int_0^R \mathrm{d}x\mathrm{d}y(xy)^4 u_{rr}(x,y) = X_\infty(R) + \widetilde{X}(R), \tag{27}$$

being

$$X_\infty\,(R) = \frac{2}{5}\sigma^2 R\int_0^R \mathrm{d}x\,\rho(x)\left[1 - \frac{5}{2}\frac{x}{R} + \frac{5}{3}\left(\frac{x}{R}\right)^2 - \frac{1}{6}\left(\frac{x}{R}\right)^5\right] \tag{28}$$

$$\widetilde{X}\,(R) = 6\,\frac{\sigma^2}{R^4}\int_0^R\int_0^R \mathrm{d}x\mathrm{d}y x^3 y^4\,\Psi\,(x,y)\,. \tag{29}$$

Similarly to the velocity covariance, the usefulness of the decomposition (27) relies on the fact that one can immediately distinguish the contribution (i.e., X_∞) to the macrodispersion due to the mean radial flow from those (i.e., $\widetilde{X}$) addressed to the fluctuations of the potential gradient. Since for $R \gg I$ the impact of fluctuations of the potential is almost exhausted (Indelman and Dagan 1999), it is reasonable to assume

$$X_{rr}(R) \approx X_\infty(R). \tag{30}$$

The approximation (30), which is shown to be accurate (see discussion in Indelman and Dagan 1999) in formations with small anisotropy ratio λ (being this latter defined as the ratio between the vertical, and horizontal correlation scale of the conductivity field K), is equivalent to neglecting into the second of (9) the term $\mathbf{E}^{(1)}(\mathbf{x}) = -\nabla\Phi^{(1)}(\mathbf{x})$, i.e.,

$$\mathbf{u}(\mathbf{x}) \approx -\frac{K_{\mathrm{A}}}{n}\varepsilon\,(\mathbf{x})\,\mathbf{E}^{(0)}\,(\mathbf{x})\,. \tag{31}$$

Nevertheless, the condition $R \gg I$ is also equivalent (for fixed R) to $I \to 0$, and therefore the approximation (30) is attached to a macrodispersion mechanism taking place in a formation characterized by a short-range correlation in the conductivity field.

However, the approximation (30) may not be appropriate either from a theoretical or from a practical standpoint. Indeed, from the theoretical point of view the approximation of Indelman and Dagan (1999) is realistic for: (i) flows generated by an infinite singular line (i.e., typically well-type flows) and (ii) taking place in highly anisotropic formations. Instead, in this case the formation is isotropic, and therefore the assumption (ii) does not apply. In addition, in most of the forced-gradient tracer experiments (see Chao et al. 2000; Fernàndez-Garcia et al. 2004; Ptak et al. 2004) breakthrough curves are monitored at distances relatively short (only a few integral scales from the injection zone). In such cases a complete evaluation of X_{rr} is required.

The computation of $X_\infty(R)$ is straightforward (see Eq. 29) once the shape of the autocorrelation ρ is assigned. Thus, it yields $X_\infty(R) = \frac{2}{5}\sigma^2 R\,\overline{X}_\infty(R)$, being

$$\overline{X}_\infty(R) = 1 - \frac{5}{2R} + \frac{10}{3R^2} - \frac{20}{R^5} + \frac{10}{R^3}\left(1 + \frac{2}{R} + \frac{2}{R^2}\right)\rho(R) \tag{32}$$

for exponential, and

$$\overline{X}_\infty(R) = \left(1 + \frac{10}{3\pi R^2}\right)\mathrm{erf}\left(\frac{\sqrt{\pi}}{2}R\right) - \frac{32}{3\pi^2 R^5} - \frac{5}{R} + \frac{2}{3\pi^2 R}\left(\frac{16}{R^4} + \frac{4\pi}{R^2} + 3\pi^2\right)\rho(R) \tag{33}$$

for Gaussian ρ, respectively. Instead, the computation of $\widetilde{X}(R)$ is achieved by means of a numerical quadrature.

We have depicted (black lines) in Fig. 3 the dimensionless scaled variance $\frac{X_{rr}(R)}{(\sigma I)^2}$ versus the normalized distance $\frac{R}{I}$ for exponential, and Gaussian ρ. As the tracer body invades the porous medium, X_{rr} increases monotonically with the distance R. At short distances X_{rr} quickly grows. Indeed, close to the source the local velocity is proportional to R^{-2}, and therefore even a small velocity fluctuation will determine a large departure from the mean trajectory (it is reminded that at the first-order in the variance σ^2 the trajectory fluctuation $\overline{X}_r'$ is proportional to the velocity fluctuation u_r). The near-field behavior can be analyzed by assuming $\rho \approx 1$ (which is a reasonable approximation in view of the assumption $R \ll I$). In such a case, the one-dimensional quadrature appearing into (14) is explicitly carried out:

$$\Psi(x,y) = \frac{1}{8x\,|x-y|}\begin{cases} \frac{1}{\sqrt{x(x-y)}}\ln\left(\frac{\sqrt{x}+\sqrt{x-y}}{\sqrt{y}}\right) + \frac{y-2x}{y^2} & x > y \\ \frac{1}{\sqrt{x(y-x)}}\left[\arctan\left(\sqrt{\frac{x}{y-x}}\right) - \frac{\pi}{2}\right] - \frac{y-2x}{y^2} & x < y, \end{cases} \tag{34}$$

and concurrently the trajectory variance is computed as $X_0(R) = a\,(I\,\sigma\,R)^2$, with

$$a = \frac{1}{9} + 6\int_0^1\int_0^1 \mathrm{d}x\mathrm{d}y\, x^3 y^4 \Psi(x,y) \simeq 0.612. \tag{35}$$

By the same token as before, it is seen that the near-field $R \ll I$ is equivalent (for given R) to $I \to \infty$, and therefore macrodispersion in the close vicinity of the source can be attached to a long-range correlation process in the K field. Thus, by assuming a long-range correlation in the conductivity field, the behavior of the second order moment close to the source is

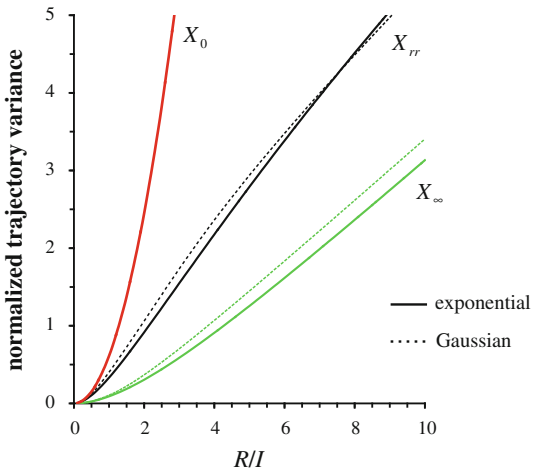

Fig. 3 Scaled trajectory variance $\frac{X_{rr}}{(\sigma I)^2}$ as function of the travel distance R/I for exponential (continuous line), and Gaussian (dashed line) autocorrelation ρ. Green lines and the red one refer to the approximation of X_{rr} in the short, and long-range correlation of K, respectively

extended to the entire domain. This explains (red curve in Fig. 3) why X_0 can be regarded as an upper bound for X_{rr}.

The far field behavior of X_{rr} can be readily studied. Indeed, at large distances the fluctuation $\overline{X}_r'$ is computed from Eq. 24 after noting that $\frac{\partial}{\partial R}\langle U(R)\rangle \approx 0$ for $R \gg I$, i.e.,

$$\frac{Q}{4\pi n}\frac{\mathrm{d}}{\mathrm{d}R}\overline{X}_r' \approx R^2 u_{\mathrm{r}}(R) \qquad R \gg I, \tag{36}$$

which leads to the following asymptotic for $\overline{X}_r'$

$$\overline{X}_r'(R) \approx \frac{4\pi n}{Q}\int_0^R \mathrm{d}x\, x^2\, u_{\mathrm{r}}(x) \qquad R \gg I. \tag{37}$$

As a consequence, the macrodispersion coefficient at large distances writes as

$$X_{rr}(R) \approx \left(\frac{4\pi n}{Q}\right)^2 \int_0^R\int_0^R \mathrm{d}x\,\mathrm{d}y\,(xy)^2\, u_{rr}(x,y) \qquad R \gg I. \tag{38}$$

Insertion of the velocity covariance (12) into (38) leads to

$$X_{rr}(R) \approx \sigma^2 \int_0^R\int_0^R \mathrm{d}x\,\mathrm{d}y\,\rho(x-y) = 2\sigma^2\int_0^R \mathrm{d}x\,(R-x)\,\rho(x). \tag{39}$$

Hence, by taking the limit $R \to \infty$, we end up with $\frac{X_{rr}(R)}{R} = \mathrm{O}(1)$. Rather than showing that X_{rr} asymptotically grows linearly with the travel distance of the mean solute front $R = R(t)$, this result is in agreement with the fact that in the far field a source-like flow (and concurrently transport) behaves as a mean uniform one (e.g., Indelman 2001; Severino et al. 2008). Inspection of Fig. 3 reveals that the linear growth is achieved for $R \geq 10\, I$. This also means that by this distance transport has reached its asymptotic (Fickian) regime. Such a finding represents an useful issue for some practical applications such as the use of tracer tests to identify the formation statistical structure. It is interesting to underline that in our case

the approximation X_∞ of Indelman and Dagan (1999) provides a systematic underestimation of X_{rr} (green lines in Fig. 3). This is explained by recalling that for isotropic formations, the use of (30) implies the neglect of the (non-zero) term $\widetilde{X}$ in (27), thus leading to a lower bound for X_{rr}.

Similar to Indelman and Dagan (1999), one can define the *apparent macrodispersivity* $\alpha^{(\mathrm{app})}(R) = \frac{1}{2}\frac{\mathrm{d}}{\mathrm{d}R}X_{rr}(R)$ as the property that, together with $\langle U(t)\rangle = \frac{\mathrm{d}}{\mathrm{d}t}R(t)$, enables one to describe transport by means of the ADE (3). The interesting result is that at large distances it yields (see Eqs. 27–29)

$$\alpha^{(\mathrm{app})}(R) = \frac{\sigma^2}{5}\int_0^R \mathrm{d}x\,\rho(x) + \mathrm{O}(R^{-1}) \qquad R \gg I. \tag{40}$$

Thus, the asymptotic apparent macrodispersivity $\alpha^{(\mathrm{app})}(\infty) = \frac{\sigma^2}{5}$ is found to be smaller as compared with the same value in transport by mean uniform flows by a factor 5. This effect is explained by the rapid change of $\langle U(t)\rangle$ during the period in which the velocities of two particles injected at the source become uncorrelated (for a wider discussion on such an issue, see Indelman and Dagan 1999).

5 Summary and Illustration of a Practical Application

The problem investigated here is that of tracer macrodispersion due to a point-like source flow in randomly heterogeneous porous media. The plume spreads due to the velocity fluctuations that are caused by the spatial variability of the conductivity K. The difficulty of such a problem stems from the fact that, unlike the common natural gradient conditions, the flow pattern is nonuniform in mean. To reduce the mathematical complexity, while keeping the most relevant features of the problem at stake, a few simplifying assumptions have been adopted. Thus, pore-scale dispersion is neglected, and a first-order approximation in the variance σ^2 of the normalized fluctuation (4) is employed to evaluate the fluid-velocity covariance. This problem was analytically tackled in the past (Indelman and Dagan 1999) by neglecting the impact of the fluctuations of the potential gradient. Such an approximation is bound to become accurate for highly heterogeneous formations, i.e., $\lambda \ll 1$.

We have computed (in closed analytical form) the second-order radial spatial moment $X_{rr}(R)$ for an isotropic (i.e., $\lambda = 1$) formation. The structure and evolution of $X_{rr}(R)$ is discussed. In particular, it is shown that it is bounded between the approximation X_∞ of Indelman and Dagan (1999), which provides a lower bound, and X_0 that represents the upper bound. While X_∞ can be attached to the macrodispersion in a formation characterized by a short-range correlation in the conductivity field, X_0 pertains to a macrodispersion mechanism taking place in a medium with a long-range correlation in the conductivity field.

To illustrate how these theoretical results can be used from a practical point of view, we consider an hypothetical heterogeneous (with $\sigma^2 = 0.5$) aquifer, and we wish showing how to characterize the heterogeneity structure by means of a divergent flow tracer test (a general discussion on such a type of field-scale tests can be found in Ptak et al. 2004). Overall, the experimental set-up requires a forcing (typically a pump) device which determines the flow field. Once steady-state conditions are met, a solute pulse (generally at constant concentration) is injected in the porous medium. Hence, *breakthrough curves* (BTC)s are monitored (at observing piezometers) at given radial distances from the release source, and matching

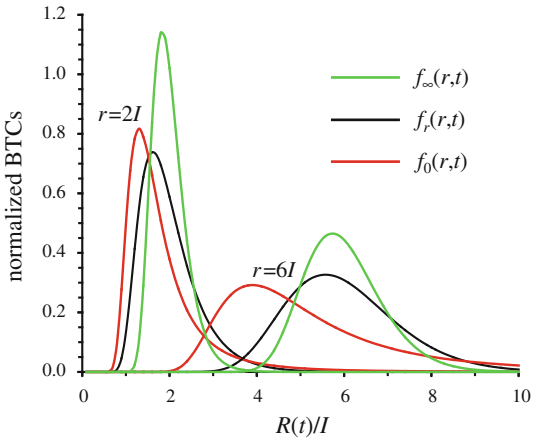

Fig. 4 Comparison between f_r (black line) with f_0 (red lines), and f_∞ (green lines) at $r = 2\,I$, and $6\,I$

over the analytical model enables one to infer the heterogeneity structure of the formation. This procedure is known as *identification problem*.

For a pulse injection, the BTC is proportional to the probability distribution function $f_r = f_r(r, t)$ of the trajectory X_r. Indeed, within the employed σ^2-approximation, the fluctuation of the particle trajectory is proportional (see Eq. 26) to the velocity fluctuation u_r, and concurrently to the normally distributed $\varepsilon(\mathbf{x})$ (second of Eq. 9). Thus, the probability density function f_r of the particle trajectory is normal, and therefore it is given by

$$f_r(r, t) = \frac{1}{[2\pi\ X_{rr}(t)]^{3/2}} \exp\left\{-\frac{[r - R(t)]^2}{2\ X_{rr}(t)}\right\}, \tag{41}$$

being $R = R(t)$ the equation of the mean front (see Fig. 1). In addition, it is reminded that X_r tends asymptotically to normality by virtue of the central limit theorem. As a consequence, Eq. 41 can be also regarded as the large distance limit of a tracer experiment out-coming. In Fig. 4 the normalized BTCs (black lines) at two (i.e., $r/I = 2; 6$) radial distances are shown. For simplicity we have dealt with exponential ρ, although the same conclusions can be drawn for Gaussian autocorrelation. For comparison purposes, we have also shown: (i) the BTCs f_0 (red lines) as computed by using X_0 and (ii) the BTCs f_∞ (green lines) that one obtains by employing the approximation of Indelman and Dagan (1999). The most evident feature is that the approximation of Indelman and Dagan (1999) leads to a systematic underestimation of the macrodispersion mechanism. Nevertheless, this was expected since $X_\infty(R) < X_{rr}(R)$ (see discussion about Fig. 3). In view of the identification problem, more interesting features can be observed from comparison with the BTCs f_0. Indeed, the formation structure authorizing the use of X_0 is that of a stratified medium with layers of decreasing thickness (see, e.g., Dagan 1989). As a consequence, fluid particles may circumvent low conducting inclusions by taking very small vertical displacements, and therefore they reach earlier the recovering zone at the piezometers. At any rate, it is worth underlying that most of the displacements are taken horizontally, thus causing a higher delay at the piezometers. This explains why the f_0-curves generally exhibit a more pronounced tail (the early arrivals notwithstanding). This simple example offers a way of readily using the theoretical results presented herein.

Before concluding, it is important to point out that in the case of statistically anisotropic formations the rate of the mean flow (and concurrently of the macrodispersion coefficient) will also depend upon on the latitudinal angle as well as by the angle between the bedding

(major axis of anisotropy) and the direction of mean flow (e.g., Gelhar and Axness 1983). These important issues, which are not considered here, serve as a warning against straightforward generalizations. Accounting for the impact of the anisotropy formation is deferred to future studies.

Acknowledgments This study was supported by the grant: Methods for monitoring, predicting and controlling soil and groundwater pollution processes due to non-point agricultural sources (# MIUR 2007WA23ZC). The author is very grateful to the three anonymous reviewers for their thorough and helpful comments which have significantly improved the early version of the manuscript.

Appendix

Derivation of Eq. 13

In order to compute the covariance $u_{l,m}(x, y)$, we first derive the covariance $C_{\varepsilon\Phi}(x, y)$. From (8) it yields

$$\Phi^{(1)}(\mathbf{x}) = \frac{Q}{K_\mathrm{A}} \int_\Omega \frac{\mathrm{d}\mathbf{x}'}{(4\pi)^2} \varepsilon\left(\mathbf{x}'\right) \frac{\mathbf{x}' \cdot \left(\mathbf{x}' - \mathbf{x}\right)}{\left(x' \left|\mathbf{x}' - \mathbf{x}\right|\right)^3}. \tag{42}$$

The cross-covariance $C_{\varepsilon\Phi}$ is calculated by multiplying $\varepsilon(\mathbf{x})$ by (42) evaluated in $\mathbf{y} \neq \mathbf{x}$, and subsequently taking the expectation to get

$$C_{\varepsilon\Phi}(\mathbf{x}, \mathbf{y}) = \frac{Q}{K_\mathrm{A}} \left(\frac{\sigma}{4\pi}\right)^2 \int_\Omega \mathrm{d}\mathbf{x}' \rho(x') \frac{\left(\mathbf{x} - \mathbf{x}'\right) \cdot \left(\mathbf{x} - \mathbf{y} - \mathbf{x}'\right)}{\left(\left|\mathbf{x} - \mathbf{x}'\right| \left|\mathbf{x} - \mathbf{y} - \mathbf{x}'\right|\right)^3}. \tag{43}$$

Switching to spherical coordinates $\left(x', \theta, \varphi\right)$ yields (after integrating over the azymuthal angle)

$$C_{\varepsilon\Phi}(x, y) = \frac{Q\sigma^2}{8\pi K_\mathrm{A}} \int_0^\infty \mathrm{d}x'\, x'^2 \rho\left(x'\right) \int_{-\pi/2}^{\pi/2} \mathrm{d}\theta\, \cos\theta \frac{x'^2 + x(x-y) - (2x-y)x' \sin\theta}{\beta(x)\beta(x-y)} \tag{44}$$

$$\beta(a) = \left(a^2 + x'^2 - 2a\, x' \sin\theta\right)^{3/2}. \tag{45}$$

Carrying out the integral over the polar angle

$$\begin{aligned} &\int_{-\pi/2}^{\pi/2} \mathrm{d}\theta\, \cos\theta \frac{x'^2 + x(x-y) - (2x-y)x' \sin\theta}{\beta(x)\beta(x-y)} \\ &= 2\frac{h\left(x'-x\right) + h\left(x'+x-y\right) - h\left(x'-x+y\right)}{\left[x'^2 - x(x-y)\right]^2} \end{aligned} \tag{46}$$

(where h is a Heaviside function defined as: $h(x) = 0$ for $x < 0$, $h(x) = 1/2$ for $x = 0$, and $h(x) = 1$ for $x > 0$), and substituting into (44), leads to:

$$C_{\varepsilon\Phi}(x, y) = \frac{\sigma^2}{\chi}\left[\int_x^\infty \frac{\mathrm{d}x' x'^2 \rho(x')}{\left[x'^2 - x(x-y)\right]^2} + \int_{-(x-y)}^\infty \frac{\mathrm{d}x' x'^2 \rho(x')}{\left[x'^2 - x(x-y)\right]^2} - \int_{x-y}^\infty \frac{\mathrm{d}x' x'^2 \rho(x')}{\left[x'^2 - x(x-y)\right]^2}\right]. \tag{47}$$

The second step consists into the computation of the potential-gradient covariance $C_{E_l E_m}$. Thus, we start with the derivation of the covariance C_Φ by employing the definition, i.e.,

$$C_\Phi(\mathbf{x}, \mathbf{y}) = \left\langle \Phi^{(1)}(\mathbf{x}) \Phi^{(1)}(\mathbf{y}) \right\rangle = \frac{Q}{K_\mathrm{A}} \int_\Omega \frac{\mathrm{d}\mathbf{x}'}{(4\pi)^2} \frac{\mathbf{x}' \cdot (\mathbf{x}' - \mathbf{x})}{(x' |\mathbf{x}' - \mathbf{x}|)^3} C_{\varepsilon\Phi}(x', y). \tag{48}$$

Like before, we switch to spherical coordinates

$$C_\Phi(x, y) = \frac{Q}{8\pi K_\mathrm{A}} \int_0^\infty \mathrm{d}x' C_{\varepsilon\Phi}(x', y) \int_{-\pi/2}^{\pi/2} \mathrm{d}\theta \cos\theta \frac{x' - x\sin\theta}{\beta(x)}, \tag{49}$$

and carry out the quadrature over the angle, i.e., $\int_{-\pi/2}^{\pi/2} \mathrm{d}\theta \cos\theta \frac{x' - x\sin\theta}{\beta(x)} = \frac{2}{x'^2} h(x' - x)$, to get

$$C_\Phi(x, y) = \chi^{-1} \int_x^\infty \frac{\mathrm{d}x'}{x'^2} C_{\varepsilon\Phi}(x', y). \tag{50}$$

The potential-gradient covariance is easily obtained from (49) after carrying out the derivatives with respect to x_l and y_m, i.e.,

$$C_{E_l E_m}(x, y) = -\chi^{-1} \frac{x_l y_m}{x^3 y} \frac{\partial}{\partial y} C_{\varepsilon\Phi}(x, y). \tag{51}$$

The velocity covariance is now written as

$$u_{l,m}(x, y) = \left(\frac{\sigma}{\chi}\right)^2 \frac{x_l y_m}{(xy)^3} \rho(|\mathbf{x} - \mathbf{y}|) - \frac{x_l y_m}{\chi x y}\left[\frac{2}{x^2}\frac{\partial}{\partial y} C_{\varepsilon\Phi}(x, y) + \frac{1}{y^2}\frac{\partial}{\partial x} C_{\varepsilon\Phi}(y, x)\right]. \tag{52}$$

Substitution of (47) into (52) leads (after carrying out the required differentiation) to (13).

References

Chao, C.-H., Rajaram, H., Illangasekare, T.H.: Intermediate scale experiments and numerical simulations of transport under radial flow in a two-dimensional heterogeneous porous medium. Water Resour. Res. **36**, 2869–2884 (2000)

Dagan, G.: Flow and Transport in Porous Formations. Springer, New York (1989)

Fernàndez-Garcia, D., Illagasekare, T.H., Rajaram, H.: Conservative and sorptive forced-gradient and uniform flow tracer tests in a three-dimensional laboratory test aquifer. Water Resour. Res. **40**, W10103.1–W10103.17 (2004). doi:10.1029/2004WR003112

Gelhar, L., Axness, C.: Three-dimensional stochastic analysis of macrodispersion in aquifers. Water Resour. Res. **19**, 161–180 (1983)
Indelman, P.: Steady-state flow in heterogeneous porous media. Transp. Porous Media **45**, 105–127 (2001)
Indelman, P., Dagan, G.: Solute transport in divergent radial flow through heterogeneous porous media. J. Fluid Mech. **384**, 159–182 (1999)
Indelman, P., Rubin, Y.: Solute transport in nonstationary velocity fields. Water Resour. Res. **32**, 1259–1267 (1996)
Indelman, P., Fiori, A., Dagan, G.: Steady flow toward wells in heterogeneous formations: mean head and equivalent conductivity. Water Resour. Res. **32**, 1975–1983 (1996)
Lessoff, S.C., Indelman, P.: Stochastic determination of three-dimensional capture zones for a fully penetrating well. Water Resour. Res. **40**, W03508.1–W03508.9 (2004). doi:10.1029/2003WR002703
Naff, R.L.: Radial flow in heterogeneous porous media: an analysis of specific discharge. Water Resour. Res. **27**, 307–316 (1991)
Ptak, T., Piepenbrink, M., Martac, E.: Tracer tests for the investigation of heterogeneous porous media and stochastic modelling of flow and transport—a review of some recent developments. J. Hydrol. **294**, 122–163 (2004)
Rubin, Y.: Applied Stochastic Hydrogeology. Oxford University Press, New York (2003)
Severino, G., Santini, A., Sommella, A.: Steady flows driven by sources of random strength in heterogeneous aquifers with application to partially-penetrating wells. Stoch. Environ. Res. Risk Assess. **22**, 567–582 (2008). doi:10.1007/s00477-007-0175-5
Shvidler, M.I.: Stochastic Hydrodynamics of Porous Media. Nedra, Moscow (in Russian) (1985)